JOURNAL OF AIRCRAFT
Vol. 45, No. 5, September–October 2008

Flow Simulation of a Supersonic Transport Configuration at Low-Speed and High-Lift Conditions

Zhong Lei*
Japan Aerospace Exploration Agency, Tokyo 181-0015, Japan

DOI: 10.2514/1.33856

The flowfield around a supersonic transport configuration with high-lift devices at a low speed and high angle of attack was investigated by solving Reynolds-averaged Navier–Stokes equations. The configuration consisted of a fuselage and a cranked arrow wing with leading- and trailing-edge flaps. Numerical simulations were conducted and validated at conditions of the wind-tunnel test. Details of the flowfield at the design condition were analyzed using computational results. The effect of the high-lift devices on aerodynamic performance was discussed. The leading-edge vortices were reduced both in size and in strength by deflecting the leading-edge flap, and the drag was reduced. The trailing-edge flap increased the effective camber of the wing and improved the lift force. A typical leading-edge vortex flap was confirmed. It was shown that the aerodynamic performance could be improved by deflecting the leading- and trailing-edge flaps.

Nomenclature

C_D	=	drag coefficient
C_L	=	lift coefficient
C_m	=	pitching moment coefficient
C_p	=	static pressure coefficient, $(p - p_\infty)/(0.5U_\infty^2)$
Cr	=	chord length of the wing root, m
c	=	local chord length of the wing, m
$\bar{c}$	=	mean aerodynamic chord (MAC), m
c_d	=	section drag coefficient
c_l	=	section lift coefficient
L/D	=	lift-to-drag ratio
p	=	static pressure
p_∞	=	freestream static pressure
p_0	=	total pressure
Re	=	Reynolds number based on $\bar{c}$ and U_∞
U_∞	=	freestream air speed, m/ sec
X	=	chordwise station from the apex of the wing root at the body center line, m
x	=	horizontal coordinate measured from the nose in the direction of the body center line, m
y	=	horizontal coordinate measured from the body center line, m
z	=	vertical coordinate measured from the x–y plane, m
α	=	angle of attack, deg
η	=	spanwise coordinate normalized by the wing semispan

I. Introduction

TYPICAL supersonic transports use a low aspect ratio and highly swept wings to reduce wave drag at supersonic cruise conditions. However, a wing with a large sweep angle of the leading edge is known for having a poor aerodynamic efficiency lift-to-drag ratio for takeoff and landing at low speeds and high angles of attack. To meet economic viability and environmental compatibility, the next generation supersonic transport (SST) is required to have sufficient low-speed performance in takeoff and landing situations [1]. For example, the first generation SST Concorde generated additional lift by encouraging vortices separated from its highly swept leading edge, and the additional vortex lift allowed Concorde to meet its takeoff and landing requirements. However, the leading-edge separation vortices also produced a large undesirable drag penalty. The additional thrust required to overcome the increased drag generated an unacceptable engine noise and large fuel consumption at the low-speed conditions. This issue has been addressed in NASA's high-speed research program [2] as well as in European supersonic civil transport research programs [3,4].

To improve aerodynamic performance of the next generation SST in takeoff and landing situations, a high-lift system is desirable to enhance the lift as well as the lift-to-drag ratio. Increased aerodynamic performance can reduce the engine power setting and therefore community noise. One approach to improve the high-lift performance of a highly swept wing at subsonic conditions is the use of a leading-edge vortex flap [5]. A suitable vortex flap locates the leading-edge vortex system on the forward facing area of a deflected flap, thus creating a low-pressure region on the flap surface and resulting in a net thrust component. The trailing-edge flap can be used to increase the effective camber of the wing and therefore the lift.

The wind-tunnel test plays an important role in the design process of an aircraft. However, the numerical simulation of high-lift flows by solving the Reynolds-averaged Navier–Stokes (RANS) equations is now used in the analysis and design of high-lift devices. It can provide details of flow structure and help the designer to understand the physics of high-lift flow. Accurate predictions of aerodynamic characteristics are required for the design of the high-lift system. Numerous experimental and computational studies of highly swept wings at low speeds and high angles of attack have been conducted over the past few decades. Brennenstuhl and Hummel [6] conducted experiments for a series of double-delta wings and provided detail discussions on the vortex structure, interaction, and breakdown. Verhaagen et al. [7] investigated the flowfield over a sharp-edged double-delta wing using both experiments and numerical computations. Gortz and Rizzi [8] computed the vortical flow over a pure delta wing and a very simple wing/body, discussed some numerical problems, and analyzed the vortex breakdown using numerical results. In NASA's high-speed research program [2], many computations have been performed to assess the accuracy of the numerical codes, and parametric studies have been conducted on high-lift systems of the high-speed civil transport configuration. As part of the European Project for the Improvement of Supersonic Transport Low-Speed Efficiency [4], a systematic study has been conducted using numerical computations for different types of leading-edge flaps of a supersonic transport configuration.

In the Japan Aerospace Exploration Agency (JAXA), a research program was started in 1996 to establish advanced technologies for the next generation supersonic transport. Within this project, one of

Received 3 August 2007; revision received 5 November 2007; accepted for publication 11 November 2007.

*Researcher, Aviation Program Group, Supersonic Transport Team, 6-13-1 Osawa, Mitaka. Member AIAA.

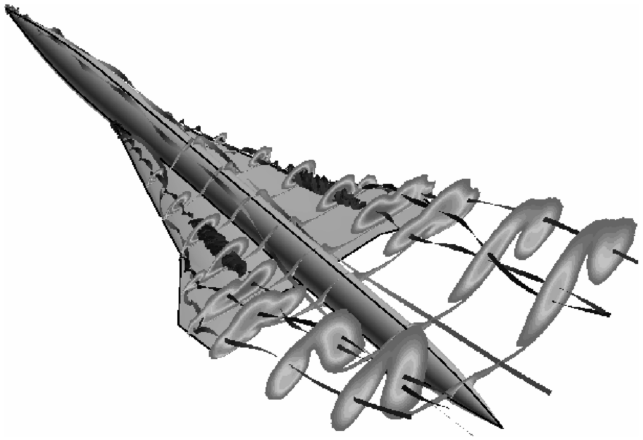

Fig. 1 Vortical flow around the SST configuration.

the fundamental studies done was to improve the aerodynamic performance at takeoff and landing conditions. Wind-tunnel tests have been conducted for a supersonic transport configuration [9]. Aerodynamic forces were measured and flow structures were investigated using an oil-flow technique and a stereoscopic particle image velocimetry survey. In parallel with the wind-tunnel testing activity, there has been a significant effort in developing the numerical modeling and simulation capabilities for the analysis and design of the SST high-lift devices. The Navier–Stokes-based computational fluid dynamics computations have been validated to accurately simulate the vortical flow over the baseline configuration [10].

The objective of this study is to investigate effect of high-lift devices on the aerodynamic performance of an SST configuration, which consists of a cylindrical body and a cranked arrow wing (Fig. 1), and to give insight into details of the flowfield at a low speed and high angle of attack (AOA). Numerical simulation is conducted to solve the compressible Reynolds-averaged Navier–Stokes equations with the turbulence model, and then compared with the experiment.

II. High-Lift System

The computational model shown in Fig. 2 is a wing–body configuration of the so-called Jet01st baseline, which was designed preliminarily for a supersonic experimental airplane in the Aerospace Aviation Program of JAXA [11]. The baseline model consisted of an axisymmetric body and a cranked arrow wing. The nose of the body was ogival and the circular cylinder had a diameter 0.1 m. The leading edge was kinked at 55% semispan station of the wing. The inboard wing was designed as a subsonic leading edge with a sweepback angle of 66 deg to reduce the wave drag at the design Mach number of 2 and an NACA66 digit series with 3–6% maximum thickness was adopted as the thickness distribution. The leading edge of the outboard wing was swept back by an angle of 42 deg to increase the aspect ratio and improve the low-speed performance. The aspect ratio of the wing was 2.42. Finally, the wing was warped by Carlson's method [12] to reduce the lift-induced drag at supersonic cruise conditions.

The leading- and trailing-edge flaps are shaded in Fig. 2. The chord lengths of the leading-edge flaps were 10% mean aerodynamic chord (MAC) for the inboard wing and 20% local chord of the outboard wing from the leading edge. The chord length of the trailing-edge flap on the inboard wing was 12.5% MAC. The trailing-edge flap was not applied to the outboard wing. The flap deflection was obtained by rotating the flap along the hinge line to the desired deflection angle. In this paper, for the sake of simplification, names of configurations are represented by a numbering system, Sxxyyzz. Here, the indices "xx," "yy," and "zz" represent deflection angles of the inboard and outboard leading- and trailing-edge flaps, respectively. For example, S301210 means that the inboard and outboard leading- and trailing-edge flaps are deflected down by 30, 12, and 10 deg. In this study, except the baseline S000000 model, four sets of inboard and outboard leading- and trailing-edge flaps are simulated. Flowfield and aerodynamic characteristics are discussed.

Experiments were carried out by Kwak et al. [13] in a low-speed wind tunnel of JAXA. Wind-tunnel tests were ranged in -4 deg $\leq \alpha \leq +30$ deg angles of attack at the air speed of freestream $U_\infty =$ 30 m/ sec and Reynolds number 0.945×10^6 based on MAC. Force and moment data were measured with an internal six-component balance system; surface pressures on the upper surface of the wing were measured at two chordwise stations of $X = 0.55Cr$, $0.83Cr$. The estimated overall uncertainties were less than $\pm 0.5\%$ for measured force coefficients C_L, C_D, and C_m, and $\pm 2\%$ for pressure coefficient C_p.

III. Numerical Simulation

In the numerical simulation, the freestream Mach number $=$ 0.088 and the $Re = 0.945 \times 10^6$ were set to match the experiment conditions. An in-house flow solver [10], the aerodynamic computational system, which was developed in JAXA's supersonic transport project, was used to simulate the flowfield and estimate the aerodynamic performance. The compressible RANS equations were discretized using a finite difference method with multiblock technique. To simulate the effect of turbulence, Menter's shear stress transport model [14] was used. It used the third-order total variation

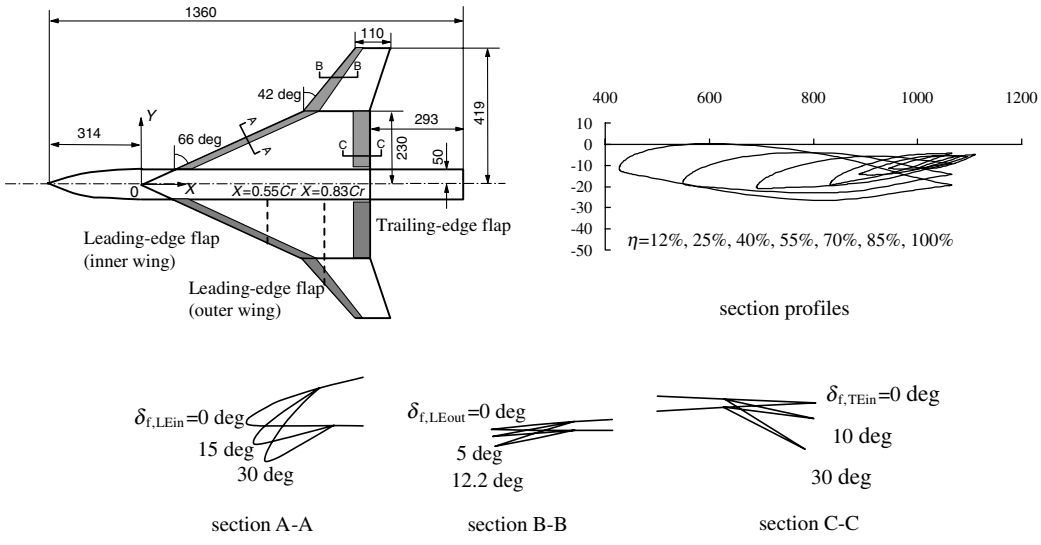

Fig. 2 The model of the SST high-lift configuration (in millimeters).

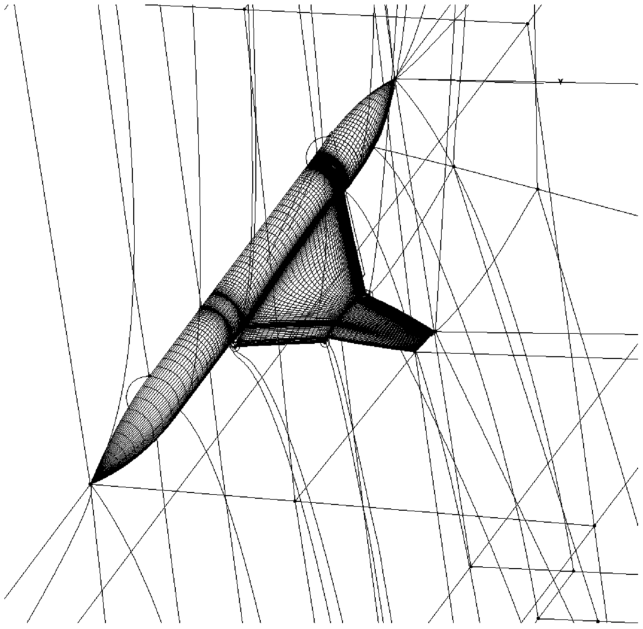

Fig. 3 Computational grids around the SST configuration.

diminishing of the Chakravarthy–Osher scheme [15] for convection terms, the central difference for other terms, and a diagonalized lower–upper decomposition method combined with the alternating direction implicit procedure for time integration. At the entrance boundary, the total pressure, total temperature, and the direction of incoming flow were specified to match the experimental conditions, whereas the velocity magnitude was obtained from the interior field by extrapolation. At the exit boundary, velocities and density were extrapolated from the interior field; only the static pressure was specified to be the reference value of the freestream. On the solid surface, the no-slip condition was applied to the velocities, and the normal derivative of pressure was forced to be zero. A symmetrical boundary condition was applied to the central plane, and a freestream condition was used on the outer boundaries of the computational region. The computation has been validated by comparing it with the corresponding experiment, and details may be found in Lei [10]. It has been shown that the Menter's model provided better results than the others.

In the computation, an ogive tail was added to the body of the wind-tunnel model to avoid simulating the support equipment in the wind-tunnel experiment. H–H topology grid systems were generated around a half model of the configuration with a 5 m width and 5 m height to model the free-air condition. Grids were extended to 3 m both upstream to the nose and downstream to the body tail. To guarantee the numerical accuracy, the spatial grid near the surface was forced normal to the configuration surface and 100 grid points were carefully distributed in the normal direction of the surface to resolve the vortex structure. The normal spacing of the first point from the surface was set to 1.0×10^{-5} MAC, corresponding to an average $y+$ of approximately 0.5. The total number of grid points is changed from 4.5 to 7.2 million for a different configuration. Computation using a coarse mesh with half of this number shows very close results. As an example, the computational mesh around the high-lift configuration, including the leading- and trailing-edge flaps, is shown in Fig. 3.

IV. Results and Discussion

Computational results for high-lift configurations will be given and compared with the experimental data. Four models, namely, S000000, S000010, S301200, and S301210, with different deflection angles of the leading- and trailing-edge flaps were simulated and analyzed. The effect of the leading- and trailing-edge flaps on the aerodynamic performance is discussed. Details of flow structure are analyzed using computational results to understand the mechanism of improvement of the aerodynamic performance. The range of lift coefficient of interest is from 0.4 to 0.8 for an SST at the low-speed region. Discussions will focus on the cases of the AOA of 12 deg, which is of interest in the design at takeoff and landing situations.

A. Aerodynamic Performance

Aerodynamic characteristics of the four models are shown in Fig. 4. The experiment shows a dependency on the deflection angle of the leading- and trailing-edge flaps. The effect of the flaps on the aerodynamic forces is well reproduced by numerical simulation. Discrepancies between the computation and the experiment are observed because of the added body tail, the assumption of fully turbulent flow, the numerical error, and the uncertainty of the turbulence model in the computation. The computation agrees well with the experiment up to the AOA of 20 deg, whereas the discrepancies become larger at high angles of attack. Small stall angles are predicted for all configurations due to the earlier vortex breakdown in the computation.

By deflecting the leading-edge flap, the leading-edge vortices are suppressed and the additional lift due to the vortex is reduced, so that the lift and the lift-α slopes of the S301200 and S301210 models are smaller than those of the S000000 and S000010 models, respectively. The stall angle is also delayed by the leading-edge flap. At lower angles of attack, the leading-edge separation is small and contributes little to the total aerodynamics forces. Because the leading-edge vortices increase the size and strength with an increase of the angle of attack, the deflection of the leading-edge flap is more effective at moderate angles of attack. Generally, the drag is changed more rapidly with the strength of the vortex than the lift, so drag reduction is larger than the reduction of the vortex lift. As a result, the aerodynamic efficiency, that is, lift-to-drag ratio (L/D), is actually improved at moderate and high angles of attack as the leading-edge flaps are deflected. The leading-edge flap has little effect on the pitching moment. On the other hand, with the deflection of the trailing-edge flap, the lift of the S000010 and S301210 models are significantly increased but the drag is larger than the S000000 and S301200 models in which the trailing-edge flap is not deflected. Because the trailing-edge flap has the effect of increasing the wing camber and increasing the suction force on the rear part of the wing, the pitching-down moment is increased. By combining the effects of the drag reduction due to the leading-edge flap and the lift increment due to the trailing-edge flap, the lift-to-drag ratio of the S301210 model is improved by more than 40% in the range of lift coefficient 0.5–0.6, which is close to the design condition of takeoff and landing situations.

The component lift and drag of the inboard and outboard wings, as shown in Fig. 5, are further calculated by using computational results. Because of the leading-edge vortex, the lift of the inboard wing is nonlinearly increased with the angle of attack. In contrast, without the leading-edge flap, the outboard wings of the S000000 and S000010 models lose their lift increment early, when the angle of attack is larger than 10 deg, and then they gradually approach stall at 20 deg. Because the outboard wing has a small sweep angle and a sharp leading edge, the stall occurs much earlier than that of the inboard wing. For the S301200 and S301210 models, the deflected leading-edge flap suppresses the leading-edge separation and has the effect of delaying the angle of attack when stall occurs. It is found that the total lift decrease due to the deflection of the leading-edge flap is mostly contributed by the inboard wing, whereas the lift of the outboard wing is slightly increased. On the other hand, drags of both the inboard and outboard wings are reduced by the leading-edge flap. It indicates that the leading-edge flap is more efficient on the outboard wing than the inboard wing at the condition of interest. The trailing-edge flap increases the drag of the inboard wing, but it has little effect on the drag of the outboard wing.

Furthermore, spanwise load distributions, which are defined as the integral of forces per unit span of the wing, are calculated. The local lift coefficient $c_l \cdot c$ and drag coefficient $c_d \cdot c$ at the AOA of 12 deg are shown in Fig. 6. As the trailing-edge flap is deflected, both the lift

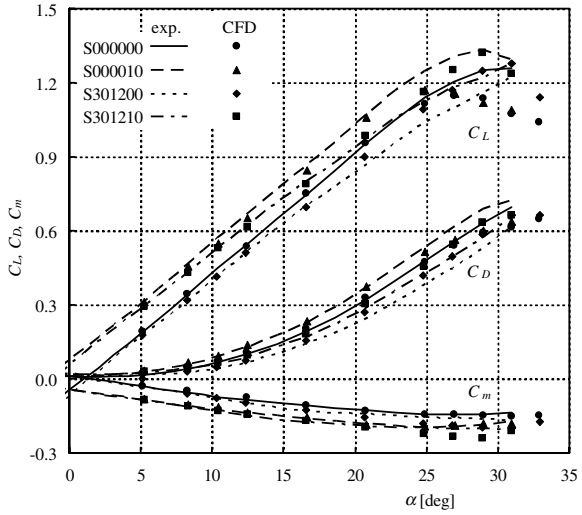

a) Lift, drag, and moment coefficients vs angle of attack

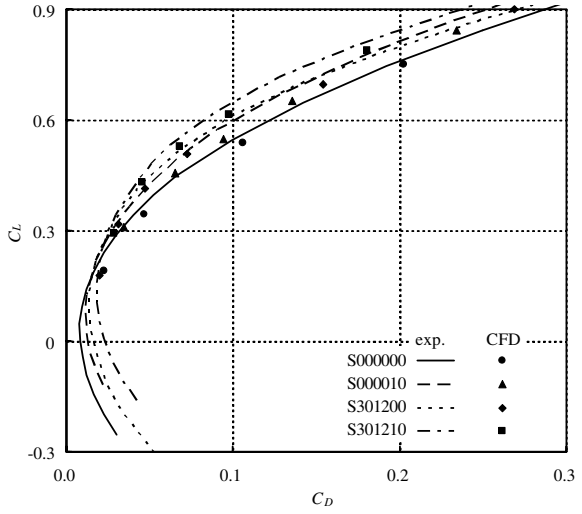

b) Lift-drag polar

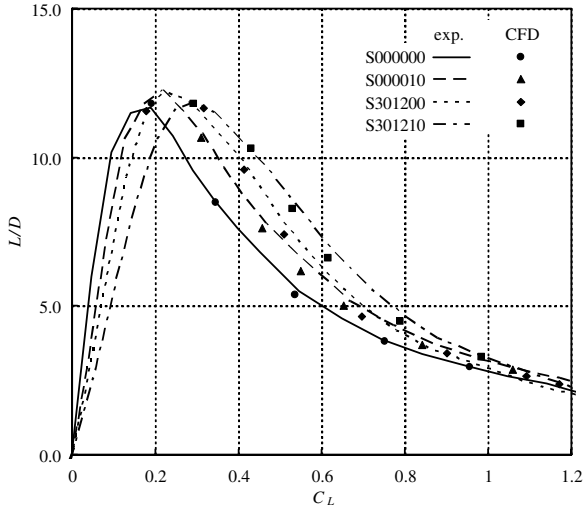

c) L/D vs C_L

Fig. 4 Aerodynamic characteristics.

and drag loads of the wing are increased. In contrast, as the leading-edge flap is deflected, both the lift and drag are decreased. The leading-edge flap is more effective on drag reduction than lift decrease. For the outboard wing, due to the delay of stall, the lift load is slightly changed, whereas the drag load is largely reduced.

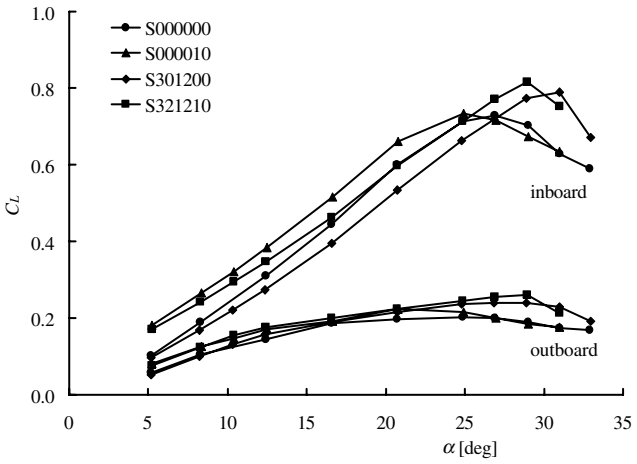

a) Lift coefficient

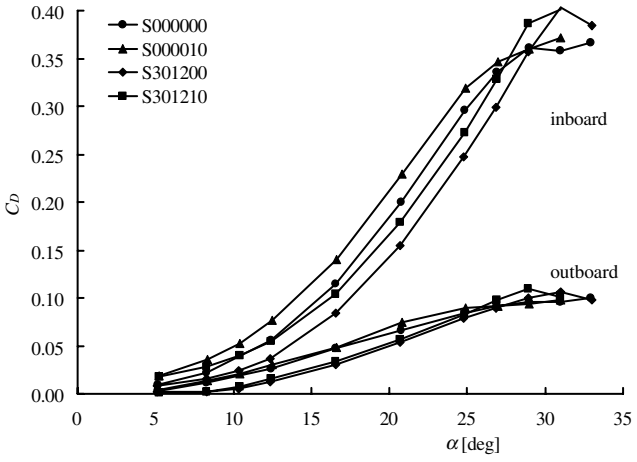

b) Drag coefficient

Fig. 5 Component contributions of aerodynamic forces.

Compared with the baseline S000000 model, the S301210 model, which combined the leading- and trailing-edge flaps, has a larger lift load and small drag load.

B. Surface Pressure

From surface pressure distributions of the computation at AOA = 12 deg in Figs. 7a and 7b, large low pressure regions due to the leading-edge primary vortices can be seen on the upper surface of the wing and generate additional vortex lift as well as drag. It shows that the leading-edge primary vortex becomes stronger with the deflection of the trailing-edge flap. In contrast, in Figs. 7c and 7d, as the leading-edge flap is deflected, on the inner wing, the leading-edge primary vortices move near to the leading edge and the low pressure region is significantly decreased. On the outboard wing, the leading-edge separation is significantly suppressed. Although the suction peak also becomes weak, the pressure of the upper surface is decreased on the whole. Therefore, the total change in the lift of the outboard wing is small. In this situation, the separation vortices are located on the upper side of the deflected leading-edge flaps, which are facing forward, thus generating low pressure regions and resulting in a net thrust component on the leading-edge flaps. At the same time, the pressure is significantly increased on the leeward side of the main wing, thus the lift and drag is decreased. With the deflection of the trailing-edge flap, as shown in Figs. 7b and 7d, the strong downwash influences the flow of not only the inboard but also outboard wings. Near the leading edge, the local angle of attack is increased and the low pressure region is enlarged a little. And so the deflection angle of the leading-edge flap with better aerodynamic performance should be also dependent on the trailing-edge flap, but

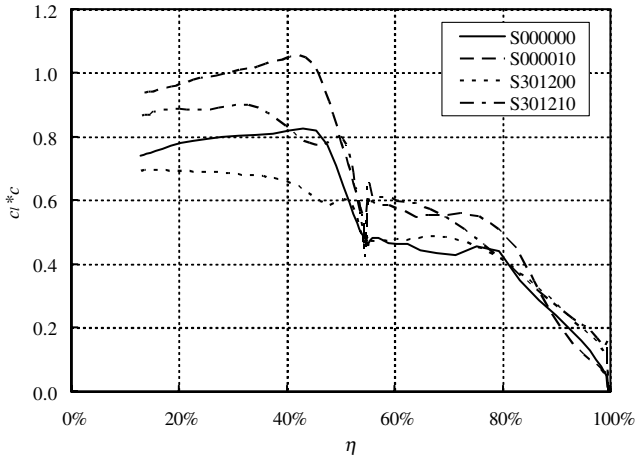

a) Section lift coefficient

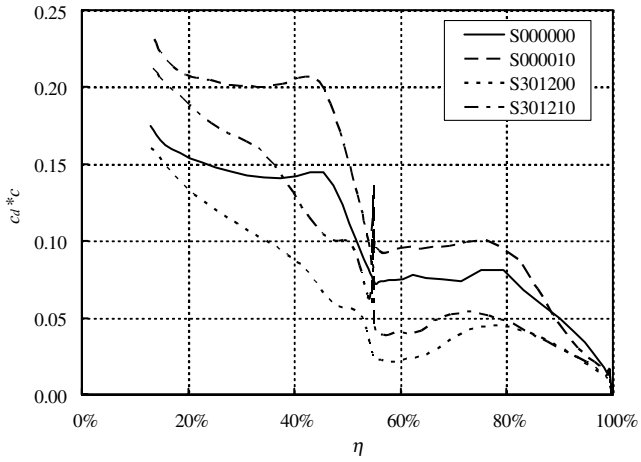

b) Section drag coefficient

Fig. 6 Spanwise load distributions at AOA = 12 deg.

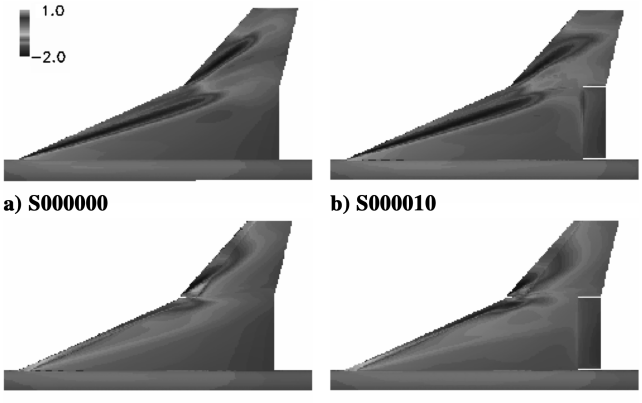

a) S000000 b) S000010

c) S301200 d) S301210

Fig. 7 Pressure distributions on the upper surface at AOA = 12 deg.

its influence is generally small. Because the deflected trailing-edge flap actually increases the camber of section airfoils, the pressure of the upper surface of the trailing-edge flap and outboard wing becomes small. Eventually, it results in an increase of the lift as well as the drag.

Pressure distributions at the two chordwise stations are compared with the experiment, as shown in Fig. 8. The computation successfully captures the main features and agrees well with the experiment. Both primary and secondary vortices are well reproduced. Higher suction peak indicates the primary vortex is

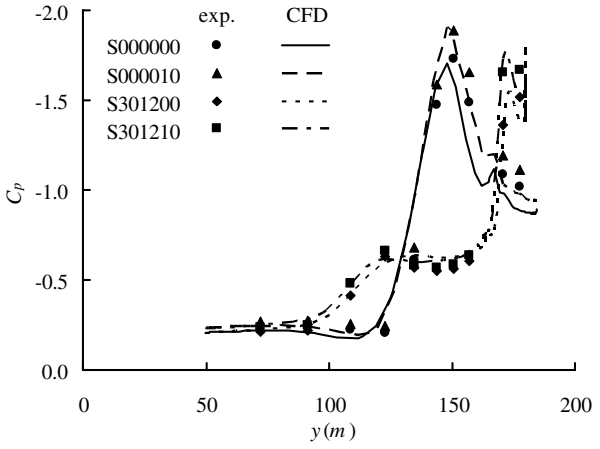

a) $X = 0.55\ Cr$

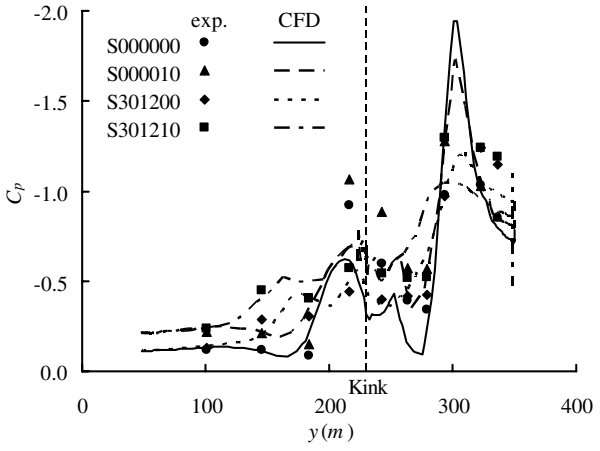

b) $X = 0.83\ Cr$

Fig. 8 Pressure coefficients on the upper surface at AOA = 12 deg.

separated from the leading edge, and the small one is due to the secondary separation vortex that is induced by the primary vortex. At the AOA of 12 deg, the pressure suction of the inboard vortex is moved to the leading edge by deflection of the leading-edge flaps, and the size of the vortex core becomes small and the suction peak of the primary vortex is reduced, as shown in Fig. 8a. Because the inboard vortex bursts further upstream from the location $X = 0.83Cr$ in the computation than that observed in the experiment, this results in a large discrepancy of pressure near the vortex from the experiment, as shown in Fig. 8b. The pressure suction becomes higher due to downwash flow induced by the deflected trailing-edge flap.

Distributions of the pressure coefficient at several spanwise stations on the surface are extracted from the computational results, as shown in Fig. 9. In all cases, in the vicinity of the leading-edge, the pressure is changed so rapidly that the strong adverse gradient results in a sudden separation. On the inboard wing (in Fig. 9a), the pressure suction peak due to the primary vortex is moved to the leading edge and the suction area becomes small. It indicates the section lift is decreased as the leading-edge flap is deflected. This results in the aforementioned lift loss. By deflecting the trailing-edge flap, the pressure is decreased on the upper surface and increased on the lower surface of the trailing-edge flap. Figure 9b shows that the trailing edge of the inboard wing also has a large influence on the outboard wing. This generated a large increase of the lift and nose-down pitching moment.

C. Flow Structure

In Fig. 10, distributions of the computed velocity magnitude at AOA = 12 deg are given at the same chordwise stations $X =$

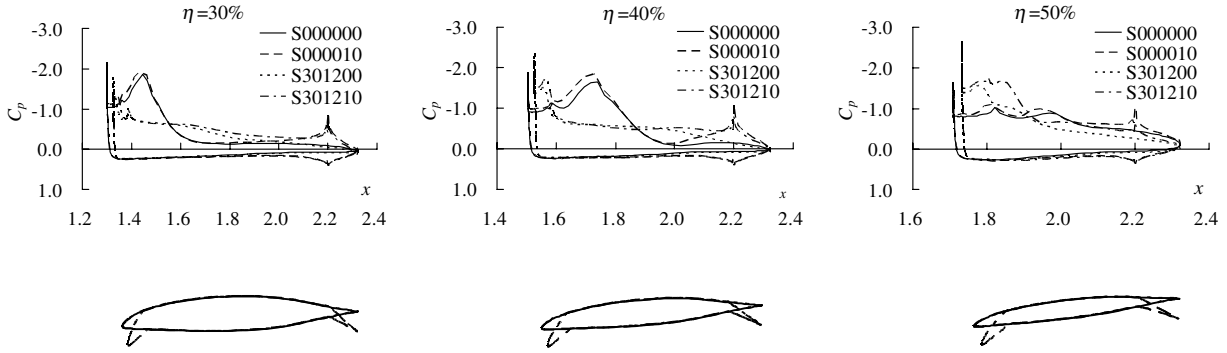

a) Inboard wing

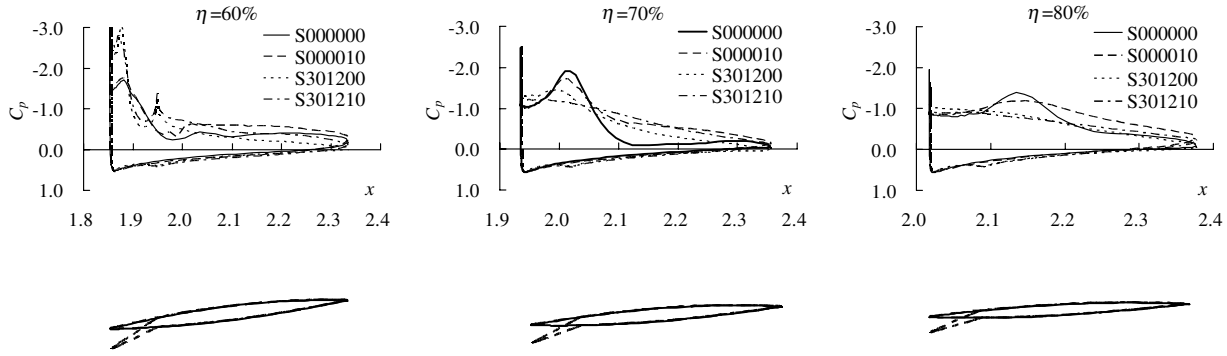

b) Outboard wing

Fig. 9 Distributions of surface pressure coefficients at different spanwise stations at AOA = 12 deg.

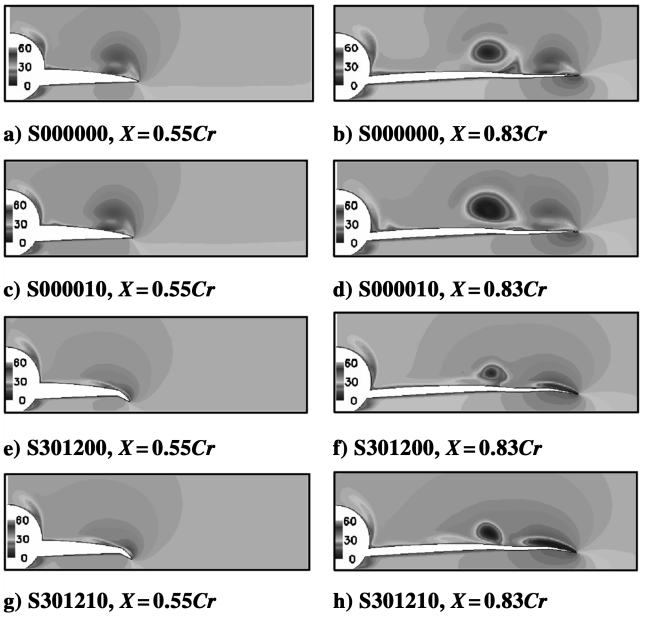

a) S000000, $X = 0.55Cr$ b) S000000, $X = 0.83Cr$

c) S000010, $X = 0.55Cr$ d) S000010, $X = 0.83Cr$

e) S301200, $X = 0.55Cr$ f) S301200, $X = 0.83Cr$

g) S301210, $X = 0.55Cr$ h) S301210, $X = 0.83Cr$

Fig. 10 Comparison of the velocity magnitude at AOA = 12 deg.

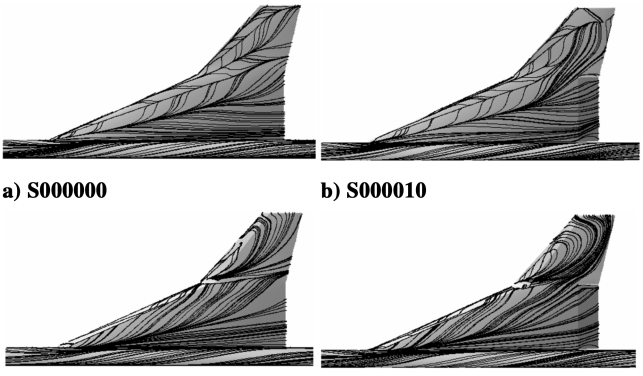

a) S000000 b) S000010

c) S301200 d) S301210

Fig. 11 Computed oil-flow pattern on the upper surface at AOA = 12 deg.

$0.55Cr$ and $X = 0.83Cr$ corresponding to Fig. 8. The leading-edge primary vortices generated on the S301200 and 301210 models are largely suppressed as compared with those of S000000 and S000010 models. As the leading-edge flap is deflected, on the upper surface of the inboard wing, the leading-edge primary vortices move toward the leading edge and the wall, and are significantly reduced in both size and strength. The vortex cores become small and weak, and the vortex breakdown is delayed. Near the leading edge, the primary vortex is restricted on the flap and generates suction forces normal to the flap. It is also found that an additional separation occurs from the hinge line of the flap on the upper surface of the inboard wing. Because the hinge line separation is very thin and weak as compared with the leading-edge one, it should not have a large influence on the aerodynamic characteristics. At the station $X = 0.83Cr$, with the deflection of the trailing-edge flap, the core of the primary vortex becomes larger and this indicates that the vortex breakdown occurs further upstream. The breakdown of the inboard vortex is prompted by the trailing-edge flap.

Computed oil-flow patterns on the wing's upper surface are shown in Fig. 11. The converged lines represent separation and the diverged ones represent reattachment. The primary and secondary vortices can be clearly identified by the limiting streamlines on the surface. The inner leading-edge vortex originates from the intersection point of

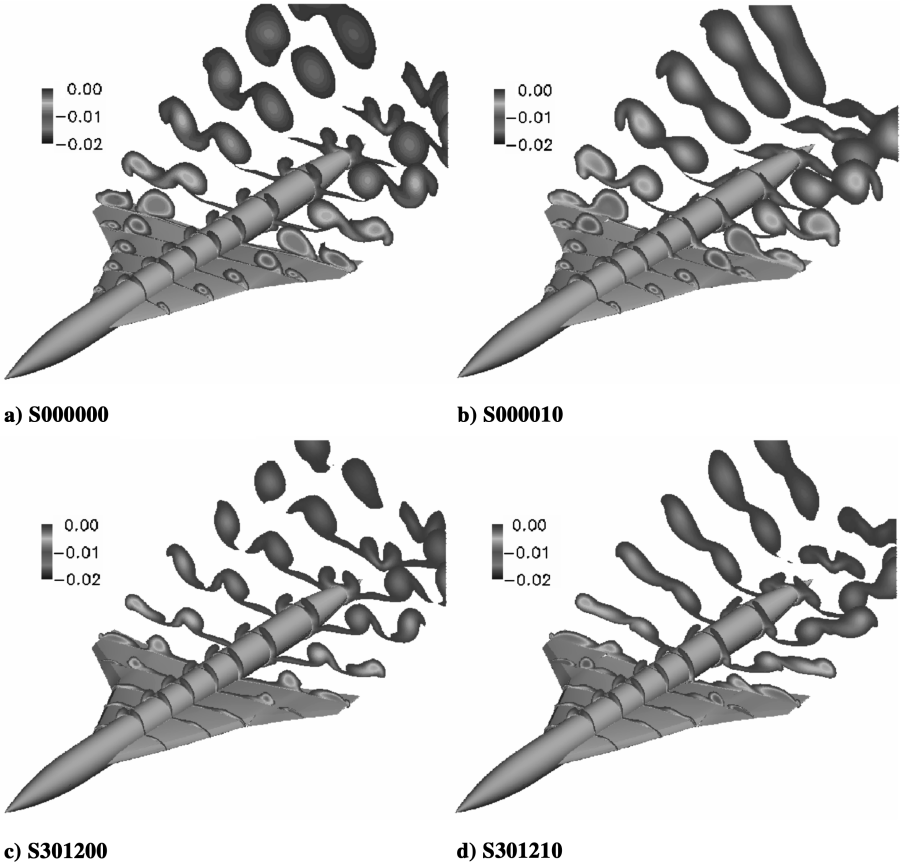

Fig. 12 Computed total pressure loss at AOA = 12 deg.

the wing leading edge and the body, whereas the outer leading-edge vortex originates from the kink, that is, the junction point of the inboard and outboard leading edge. For the S000000 (Fig. 11a) and S000010 (Fig. 11b) models, the flow is separated a little downstream from the leading edge and then reattached later on the wing's upper surface. Finally, the primary vortex is formed with a large separation region, thus generating additional vortex lift and drag. The reattachment line of the inboard primary vortex is eventually diverged from a point downstream to the kink, and this indicates a physical phenomenon of vortex breakdown. By deflecting the leading-edge flap, like the S301200 (Fig. 11c) and S301210 (Fig. 11d) models, it makes the primary vortex reattach shortly on the surface of the leading-edge flap. The secondary vortex disappears because the suppressed primary vortex is not strong enough to make the boundary layer separate. The inboard leading-edge primary vortex is completely located on the flap and bent downward at the leading-edge kink. As the trailing-edge flap is deflected, for the cases of leading-edge flap deflection, in Figs. 11c and 11d, a separation line along the hinge line of the leading-edge flap can be distinguished on the upper surface of the inboard wing, and the corresponding reattachment line is close to the body. The crossflow due to the hinge line separation is much weaker than that induced by the leading-edge primary vortex shown in Figs. 11a and 11b. On the outboard wing, because the separation is largely suppressed by the leading-edge flap, most of the primary vortex is restricted to the upper surface of the leading-edge flap. It is clearly seen that both leading-edge vortices of the inboard and outboard wings are located on the flap's upper surface, and a typical vortex flap described by Rao [5] is achieved at this flap deflection.

In the present cases, the viscous effect in the boundary layer and separation vortex is the only factor that accounts for the loss in total pressure. In Fig. 12, distributions of total pressure loss $(p_{0,\infty} - p_0)/p_{0,\infty}$ are shown at several chordwise stations. The larger the separation, the more the loss in total pressure. It can be seen that both the inboard and outboard leading-edge vortices are continuously fed with vorticity by separated shear layer from the leading edge, bent at the kink and wing tip, respectively, and eventually convects longitudinally downstream. As the leading-edge flaps are deflected, the level of total pressure loss is reduced, and less total pressure is lost. As a result, the drag is reduced. Conversely, the trailing-edge flap makes the vortex large in strength and size, thus the drag due to the vortex is increased. The combination of leading- and trailing-edge flaps has the smallest total pressure loss and is the most efficient.

V. Conclusions

Flow around a supersonic transport configuration with high-lift devices has been investigated at low-speed conditions by numerical simulation. The Reynolds-averaged Navier–Stokes equations were solved and the computational results were used to analyze the details of the flowfield. It was confirmed that the leading- and trailing-edge flaps had the effect of improving the aerodynamic performance from the baseline configuration. Major conclusions are summarized as follows.

1) As the leading-edge flap is deflected, both the lift and drag of the inboard wing is decreased, whereas for the outboard wing, the lift is enhanced and the drag is reduced due to the delay of the stall. With the increase of the flap deflection, the leading-edge vortex is reduced in both size and strength. At a large deflection, the leading-edge vortices are located on the flap's upper side, and a typical vortex flap is confirmed.

2) The trailing-edge flap increases the effective camber of the wing, and the pressure is decreased on the upper surface and increased on the lower surface of the trailing-edge flap. It generates a large increment of the lift and nose-down pitching moment.

3) The combination of leading- and trailing-edge flaps has the advantage of increasing the lift and reducing the drag at the same time. It greatly improves the lift-to-drag ratio by more than 40% at the lift coefficient $C_L = 0.5$–0.6.

4) Validation shows that the numerical simulation provides an accurate prediction of the aerodynamic characteristics and captures the flow features reasonably well, compared with the experiment.

Acknowledgments

The author would like to thank D. Y. Kwak for providing the experimental data and F. Kuroda for his help with grid generation.

References

[1] Antani, D. L., and Morgenstern, J. M., "HSCT High-Lift Aerodynamic Technology Requirements," AIAA Paper 92-4228, Aug. 1992.

[2] "1998 NASA High-Speed Research Program Aerodynamic Performance Workshop," *High Lift*, CP-1999-209704, edited by D. E. Hahne, Vol. 2, NASA, Feb. 1999.

[3] Lovell, D. A., "European Research to Reduce Drag for Supersonic Transport Aircraft," AIAA Paper 99-3100, June 1999.

[4] Herrmann, U., "Low-Speed High-Lift Performance Improvements Obtained and Validated by the EC-Project EPISTLE," Institute for Computer Applications in Science and Engineering Paper 2004-411, 2004.

[5] Rao, D. M., "Exploratory Subsonic Investigation of Vortex Flap Concept on Arrow-Wing Configuration," NASA Paper CP-2108, 1980.

[6] Brennenstuhl, U., and Hummel, D., "Vortex Formation over Double-Delta Wings," International Council of the Aeronautical Sciences Paper 82-6.6.3, 1982.

[7] Verhaagen, N. G., Jenkins, L. N., Kern, S. B., and Washburn, A. E., "A Study of the Vortex Flow over a 76/40-deg Double-Delta Wing," AIAA Paper 95-0650, Jan. 1995.

[8] Gortz, S., and Rizzi, A., "Computing the High-Alpha Aerodynamics of Delta Wings—Evaluation and Analysis," AIAA Paper 2001-0015, Jan. 2001.

[9] Kwak, D. Y., Rinoie, K., and Noguchi, M., "Experimental Research of Aerodynamics on an SST Configuration with High Lift Devices," International Council of the Aeronautical Sciences Paper 2006-5.11.3, Sept. 2006.

[10] Lei, Z., "Effect of RANS Turbulence Models on Computations of Separated Flows over a Wing-Body Configuration," *Transactions of the Japan Society for Aeronautical and Space Sciences*, Vol. 48, No. 161, 2005, pp. 152–160.
doi:10.2322/tjsass.48.152

[11] Yoshida, K., and Makino, Y., "Aerodynamic Design of Unmanned and Scaled Experimental Airplane in Japan," European Community on Computational Methods in Applied Sciences, Jyväskylä, Finland, July 2004.

[12] Carlson, H. W., and Miller, D. S., "Numerical Methods for the Design and Analysis of Wings at Supersonic Speed," NASA TN D-7713, 1973.

[13] Kwak, D., Miyata, K., Noguchi, M., Sunada, Y., and Rinoie, K., "Experimental Investigation of High Lift Device for SST," National Aerospace Laboratory TR-1450, 2002.

[14] Menter, F. R., "Zonal Two Equation k–ϵ Turbulence Models for Aerodynamic Flows," AIAA Paper 93-2906, June 1993.

[15] Chakravarthy, S. R., and Osher, S., "A New Class of High Accuracy TVD Schemes for Hypersonic Conservation Laws," AIAA Paper 85-0363, Jan. 1985.